Dynamic Light Scattering and Optical Absorption Spectroscopy Study of pH and Temperature Stabilities of the Extracellular Hemoglobin of *Glossoscolex paulistus*

Patrícia S. Santiago,*† Franciane Moura,* Leonardo M. Moreira,* Marco M. Domingues,† Nuno C. Santos,† and Marcel Tabak*

*Instituto de Química de São Carlos, Universidade de São Paulo, São Paulo, Brazil; and †Unidade de Biomembranas, Instituto de Medicina Molecular, Faculdade de Medicina da Universidade de Lisboa, Lisbon, Portugal

ABSTRACT The extracellular hemoglobin of *Glossoscolex paulistus* (HbGp) is constituted of subunits containing heme groups, monomers and trimers, and nonheme structures, called linkers, and the whole protein has a minimum molecular mass near 3.1×10^6 Da. This and other proteins of the same family are useful model systems for developing blood substitutes due to their extracellular nature, large size, and resistance to oxidation. HbGp samples were studied by dynamic light scattering (DLS). In the pH range 6.0–8.0, HbGp is stable and has a monodisperse size distribution with a *z*-average hydrodynamic diameter (D_h) of 27 ± 1 nm. A more alkaline pH induced an irreversible dissociation process, resulting in a smaller D_h of 10 ± 1 nm. The decrease in D_h suggests a complete hemoglobin dissociation. Gel filtration chromatography was used to show unequivocally the oligomeric dissociation observed at alkaline pH. At pH 9.0, the dissociation kinetics is slow, taking a minimum of 24 h to be completed. Dissociation rate constants progressively increase at higher pH, becoming, at pH 10.5, not detectable by DLS. Protein temperature stability was also pH-dependent. Melting curves for HbGp showed oligomeric dissociation and protein denaturation as a function of pH. Dissociation temperatures were lower at higher pH. Kinetic studies were also performed using ultraviolet-visible absorption at the Soret band. Optical absorption monitors the hemoglobin autoxidation while DLS gives information regarding particle size changes in the process of protein dissociation. Absorption was analyzed at different pH values in the range 9.0–9.8 and at two temperatures, 25°C and 38°C. At 25°C, for pH 9.0 and 9.3, the kinetics monitored by ultraviolet-visible absorption presents a monoexponential behavior, whereas for pH 9.6 and 9.8, a biexponential behavior was observed, consistent with heme heterogeneity at more alkaline pH. The kinetics at 38°C is faster than that at 25°C and is biexponential in the whole pH range. DLS dissociation rates are faster than the autoxidation dissociation rates at 25°C. Autoxidation and dissociation processes are intimately related, so that oligomeric protein dissociation promotes the increase of autoxidation rate and vice versa. The effect of dissociation is to change the kinetic character of the autoxidation of hemes from monoexponential to biexponential, whereas the reverse change is not as effective. This work shows that DLS can be used to follow, quantitatively and in real time, the kinetics of changes in the oligomerization of biologic complex supramolecular systems. Such information is relevant for the development of mimetic systems to be used as blood substitutes.

INTRODUCTION

Giant extracellular hemoglobins, also known as erythrocruorins, have been investigated as a model of extreme complexity in oxygen-binding heme proteins (1–3). They are characterized by a very high molecular mass and their oligomeric structure together with the crowded and protected heme envinronment are two of the main factors responsible for the high redox stability. Superoxide-dimustase-like intrinsic activity, observed for hemoglobins of *Lumbricus terrestris* (HbLt) and *Arenicola marina*, is another important factor (1,4). These hemoglobins present a highly cooperative oxygen binding and a peculiar behavior associated with their oligomeric dissociation into smaller subunits and possible rearrangement back into the native oligomeric structure (5,6).

The giant extracellular hemoglobin of *Glossoscolex paulistus* (HbGp) is characterized by a minimum molecular mass of 3.1×10^6 Da (7), being constituted by a large number of subunits containing heme groups with molecular masses in the range 15–19 kDa. These heme-containing subunits form monomers of 16 kDa (*d*) and heterotrimers of 51–52 kDa (*abc*), linked by nonheme structures (24–32 kDa) called linkers (3,8,9). A recent partial characterization of molecular mass of HbGp confirmed the similarity of its subunits to those of homologous proteins of this class, described above (10). This characteristic multisubunit content confers on the whole protein a double-layered hexagonal oligomeric structure (8,11). A common model for the quaternary structure, the so-called ''bracelet model'', has been employed to explain the assembly of this class of proteins into their oligomeric structure (9). It is worthy of note that HbGp belongs to the same class of hemoglobins as HbLt, which is one of the most studied hemoglobins in this group (12–19). Due to their

Submitted July 5, 2007, and accepted for publication October 25, 2007.

Address reprint requests to Marcel Tabak, Instituto de Química de São Carlos, Universidade de São Paulo, São Paulo, Brazil. Tel.: 55-16-33739979; Fax: 55-16-33739985; E-mail: marcel@sc.usp.br.

Leonardo M. Moreira's present address is Instituto de Pesquisa e Desenvolvimento, Universidade do Vale do Paraíba, São José dos Campos, São Paulo, Brazil.

Editor: Jill Trewhella.

0006-3495/08/03/2228/13 $2.00

doi: 10.1529/biophysj.107.116780

extracellular nature, large size, and resistance to oxidation, erythrocruorins have been proposed as useful model systems for developing therapeutic extracellular blood substitutes, and preliminary animal experiments have been encouraging (4). Studies focused on the giant extracellular hemoglobin of *Arenicola marina* have shown excellent possibilities for application of this protein as artificial blood. This hemoglobin is easily available and can be purified to a homogeneous product, avoiding costly synthetic steps. Since cell membranes are not present and the protein is not glycosylated, hexagonal bilayer hemoglobins are easy to store, their side effects are less pronounced, and they are less likely to cause immunogenic responses. Furthermore, recombinant DNA techniques can be used to express the hemoglobin at large quantities (4).

Dynamic light scattering (DLS) has also been successfully applied to monitor changes in the molecular size of proteins upon denaturation and dissociation (20). Kinetic experiments play an essential role in these investigations, especially in the detection of intermediate states. Until now, kinetic data were mostly obtained by other spectroscopic methods. It is a matter of interest that DLS can provide direct access to protein size and shape data either by measuring the radius of gyration using small-angle x-ray scattering or by using the Stokes radius obtained by DLS. DLS measurements of time-dependent processes have been reported for some biomacromolecular systems. Some examples of such systems are the aggregation of insulin molecules (20), changes of the size distribution (21,22), and protein aggregation (23). The time constants for these processes were of the order of minutes, hours, or days.

Kinetic studies focusing on the hemocyanin from *Octopus vulgaris* have been developed with the aim to better understand the dissociation process mechanisms (24). Analyzing different dissociation models, the authors concluded that the best model is described by the dissociation of decamers to monomers in three consecutive and irreversible steps, with a highly cooperative step associated with the dissociation of octamers to dimers, which were assumed as the single intermediate species. Evidence for intermediate steps comes from the observation of a triple exponential decay. This study was performed using a Bio-Logic stopped flow system, and the time dependence of the 450-nm static light scattering intensity, scattered at 90°, was monitored (24).

A study of amelogenin self-assembly, using DLS as a function of temperature and at acidic pH (25), is also worthy of notice. The influence of temperature and protein concentration on the aggregation of amelogenin nanospheres at high protein concentrations was analyzed with a view to obtaining insights into the mechanism of amelogenin self-assembly to form higher-order structures.

In this work, the dissociation and denaturation of HbGp in the oxy form were studied at different pH values and as a function of temperature. This study was conducted using DLS to investigate changes produced in the protein structure upon both alkaline dissociation and increase of temperature. Characterization by electronic optical absorption spectra in the ultraviolet-visible (UV-Vis) and gel exclusion chromatography experiments was performed to complement the DLS data. At pH 7.0, a high stability of the native form of oxy-HbGp is observed, whereas at pH 9.0, an intense dissociation of the oligomer is promoted by alkalization (26). Oligomeric dissociation is an important factor enhancing the autoxidation process, since separation of the subunits would allow higher solvent accessibility to the heme, as compared to the native nondissociated form. The contact between solvent molecules and the ferrous coordination center is crucial for the autoxidation rates, since the large hydrophobic character of the native heme pocket is responsible for the redox stability of the heme (26,27). UV-Vis spectroscopy studies are used to characterize the autoxidation in the pH range 9.0–9.8 while DLS results give support, to monitor the kinetics of oligomeric dissociation as a function of pH, as well as temperature stability, of HbGp.

Therefore, the effects of two important factors, pH changes and temperature variation, on the HbGp oligomeric structure, are evaluated. The dissociation and autoxidation of HbGp are studied, varying the pH values from neutral, pH 7.0, to alkaline, pH 10.7, and increasing the temperature from 20°C to 65°C. New insights are obtained regarding pH- and temperature-induced dissociation of HbGp and also on the temperature stability of the protein. On the basis of these investigations, the usefulness of kinetic DLS measurements is demonstrated.

MATERIALS AND METHODS

Sample preparation

Glossoscolex paulistus annelid is prevalent in sites near Piracicaba, Araras, and Rio Claro, cities in the state of São Paulo, Brazil. HbGp was prepared using freshly drawn blood from worms collected in the soil from Piracicaba fields, generally 24 h before the extraction (28,29). The hemoglobin was extracted after anesthetizing the animal with ether for a period of 15–20 min. An incision was made in the upper part of the animal to avoid the digestive enzymes, and the blood was collected with a Pasteur pipette using sodium citrate as an anticoagulant. The collected blood was maintained in ice. The blood sample (HbGp) was prepared by a centrifugation at 4°C (5000 rpm for 15 min) to eliminate cell debris, followed by an ultrafiltration (molecular mass cutoff 30 kDa) and ultracentrifugation at 250,000 $\times$ g at 4°C for 6 h. The protein is obtained as a pellet, then resuspended in a minimum of 0.1 M Tris-HCl buffer, pH 7.0, and stored in the oxy-form at 4°C. Chromatography at pH 7.0 in a Sephadex G-200 column furnished the samples used in our experiments. All concentrations were determined spectrophotometrically using the molar extinction coefficient $\varepsilon_{415\text{nm}} = 5.4\ (\text{mg/ml})^{-1}\ \text{cm}^{-1}$ (28,29). Samples used for optical absorption and DLS had a protein concentration of 0.5 mg/ml. The solutions were prepared by diluting the stock HbGp concentrated solution in acetate-phosphate-borate 30-mM buffers with different pH values. The buffer and protein solutions were purified through filters of pore size 0.45 μm (Whatman, Florham Park, NJ) directly into the scattering cells. pH values were checked before and after each experiment. The purity of the native protein is assessed from the extremely narrow band obtained in Sephadex G-200 gel filtration at pH 7.0. Additional gel filtration experiments were performed for samples of HbGp at 6.0 mg/ml protein, incubated at three different pH values, 7.0, 9.0, and 9.6. Separations were performed in a similar way as in the protein purification described above, using a glass column of diameter 0.9 cm by length 90 cm, and collecting 0.9-ml samples with an

ISCO fraction collector (Louisville, KY). To assess the nature of the fractions obtained in these experiments, light scattering intensity (LSI) was measured in a spectrofluorimeter (F-4500, Hitachi, Tokyo, Japan), using both excitation and emission wavelengths at 350 nm (27).

Dynamic light scattering

DLS analyzes the fluctuations of the scattering light. The fluctuation rate is related to the diffusion coefficient of the scattering species. The radius of a hard sphere with the same diffusion coefficient is the hydrodynamic radius, R_h. Additional radii, such as the rotation radius, a mass radius, and a radius of gyration are also defined. Molecules in solution are undergoing constant diffusion. This diffusion is the result of thermal fluctuations in the suspension (Brownian motion). The diffusion coefficient is related to the size of the diffusing object (30). A spherical particle with radius R_h in a medium of viscosity η and at temperature T will diffuse with a diffusion coefficient, D, given by the Stokes-Einstein equation (30):

$$D = \frac{kT}{6\pi\eta R_h}. \quad (1)$$

If the diffusion coefficient is measured and the viscosity of the solvent is known, then the hydrodynamic radius can be calculated from the previous equation. For a spherical particle, the hydrodynamic radius is the effective size of the molecule as detected by its diffusion.

DLS measurements were performed using a noninvasive back-scatter (NIBS) apparatus (Malvern Nano ZS, Malvern, UK) with a constant 173° scattering angle, at 25°C ± 0.1°C. In this equipment, corrections can be made for the inner filter at He-Ne laser wavelength $\lambda = 633$ nm. Back-scatter measurement reduces interference from multiple scattering, as the light beam does not have to travel through the entire sample solution and thus allows higher-concentration solutions to be analyzed. It also limits the interference from dust particles, which behave as large particles and do not scatter significantly in the backward direction. The sample volume used for analysis was 2 ml. All the samples presented an absorption at 633 nm <0.01. The scattering intensity data were processed using the instrumental software to obtain the hydrodynamic diameter (D_h) and the size distribution of scatterers in each sample. The instrument measures the time-dependent fluctuation in intensity of light scattered from the particles in solution. Malvern's DTS software analyzes the acquired correlogram (correlation function versus time plot) for the calculation of D_h. Hydrodynamic diameters of the particles were estimated from the autocorrelation function, using the Cumulants method. In a typical size distribution plot from the DLS measurement, the x axis shows a distribution of size classes (nm) and the y axis shows the relative intensity of the scattered light. This is therefore known as an intensity distribution plot. A total of 15 scans with an individual duration of ~5 min were obtained for each sample. All samples were analyzed in triplicate.

DLS melting curves

Proteins are charged biomolecules that can fold into compact structures that are very sensitive to solution conditions. As an extreme case, thermal denaturation can lead to irreversible loss of structure and function of the biomolecule. Thermal denaturation typically leads to an increase in size that can be monitored by dynamic light scattering. At the protein melting point, a marked increase in hydrodynamic size and scattering intensity is observed. This protein melting point temperature is indicative of the thermal stability of a protein. Modifications such as dissociation and/or denaturation can influence the stability and are easily observed using dynamic light scattering.

Many proteins show profound changes when exposed to extreme solution conditions, with the most pronounced structural change being thermal denaturation. When a protein is heated above its characteristic thermal stability point (protein melting point), significant unfolding leads to exposure of hydrophobic chains and can cause severe, nonreversible aggregation. Light scattering is ideal for studying the protein melting point phenomenon, as the technique is extremely sensitive to large scattering objects such as aggregates and denatured protein. Similar structure changes may occur over time, pH, ionic strength, and various other solution conditions, and light scattering, again, is an ideal tool to quickly assess the condition of the molecule in solution (31).

An automated temperature scan of the sample chamber allows observation of both the size and the scattering intensity as a function of temperature. The marked point where both the size and the intensity start to increase significantly is called the melting point. Measurements of the melting point were carried out using the DLS equipment described above. The solutions were placed in the thermostatted sample chamber that was temperature-regulated for measurements over the interval 20–65°C. The temperature was controlled with an accuracy of ±0.1°C. The temperature change of 1°C is achieved in 5 min, and at each temperature, data are taken during a 15-min interval. Thus, for each temperature, an experimental time of 20 min is used. The speed of temperature change corresponds to 3°C/h.

Determination of rate constants using DLS measurements

Many different kinetic models of dissociation are possible. Among them, only those that have analytical solutions have been considered for comparison with the experimental traces. This is obtained when all steps in the process are assumed to be irreversible, and the analytical solutions turn out to be sums of exponential terms. Thus, the most general model, considered by us, is characterized by alkaline dissociation of the dodecamer into the tetramer, followed by dissociation of the tetramer into trimer and monomer:

$$\mathrm{HbGp} \rightleftharpoons 12(abcd)_3\mathrm{L}_3 \quad (2)$$

$$12(abcd)_3\mathrm{L}_3 \rightleftharpoons 36(abcd) + 36\mathrm{L} \quad (3)$$

$$36(abcd) \rightleftharpoons 36(abc) + 36(d), \quad (4)$$

where HbGp stands for the native protein, $(abcd)_3L_3$ corresponds to 1/12 of the whole protein, $(abcd)_3$ to a dodecamer, $(abcd)$ to a tetramer, (abc) to a trimer, and (d) to a monomer. This assumption is made on the basis of recent partial characterization of the molecular masses of HbGp subunits by matrix-assisted laser-desorption-ionization time-of-flight mass spectrometery (MALDI-TOF MS), where the existence of monomer, trimer, and linker subunits was observed (10). It is consistent with the reported equilibria observed in gel filtration experiments for HbLt (5,6). Since there are no similar data yet available for HbGp, our model should be regarded as an approximation, probably requiring future improvements. It is simply the first model that can be used on the analysis of oligomeric dissociation. Based on the model described by Eqs. 2–4, an overall equation for the kinetics of dissociation was deduced to fit the experimental data of average diffusion coefficient, D_Z, as a function of time:

$$D_Z = \frac{(M_p^2 D_p - BD_\infty)e^{-kt} + BD_\infty}{(M_p^2 - B)e^{-kt} + B}. \quad (5)$$

The derivation of this equation and definition of parameters are presented in the Appendix.

Determination of rate constants of autoxidation using UV-Vis measurements

To obtain the rate constants of HbGp autoxidation, the absorbance at 415 nm (A_{415}) was monitored over time. The protein concentration was 0.5 mg/ml, the same as for DLS studies. The oxy-HbGp was monitored from the characteristic relative intensities for the Q-bands (29). The collected data were

fitted to a combination of first-order kinetics with two rate constants, characterizing a fast and a slow process as described in Poli et al. (26):

$$A_t = \Delta A_{max1}\exp(-k_{obs1}t) + \Delta A_{max2}\exp(-k_{obs2}t) + A_\infty. \quad (6)$$

In this equation, A_t is the absorbance at time t and A_∞ is the absorbance at infinite time; k_{obs1} and k_{obs2} represent first-order rate constants for the fast and slow autoxidation processes, respectively; and ΔA_{max1} and ΔA_{max2} are the variation of absorbance ($A_{t=0} - A_\infty$), which correspond to the total oxidation of the rapidly- and slowly-reacting hemes, respectively. The autoxidation of the native hemoglobin, depending on the solution pH and temperature, required either a combination of two exponentials or a monoexponential fit (26). Three independent experiments were carried out for each condition.

RESULTS AND DISCUSSION

DLS

The *z*-average diameter is the mean diameter of the ensemble of particles, and is derived from the slope of the linearized form of the correlation function. Fig. 1 shows the light scattering data (*z*-average hydrodynamic diameter, $\langle D_h \rangle$) of the oxy-HbGp at different pH values as a function of time. In the pH range between 4.8 and 8.0 the protein is in its native oligomeric and integer form, showing a high stability (Fig. 1 *A*). The z-average diameter, followed for 72 h, was 27 ± 1 nm at 25°C. Under these experimental conditions, the high stability of the oligomeric protein was confirmed and the particle size was not modified (Fig. 1 *A*). It is worthy of notice that in Fig. 1 *A* data are shown for the samples monitored for 1.5 h. Measurements at longer times (up to 72 h) were performed for these samples. Table 1 summarizes the DLS results obtained at different pH values. In the pH range 4.8–8.0, the $\langle D_h \rangle$ values are obtained for a time interval of 1.5 h, whereas for pH >9.0, the values correspond to the end of kinetics, that is to the linear region where there is no significant variation with time (last 1.5 h in the kinetics shown in Fig. 1 *C*). The transition to more alkaline pH values, above pH 8.0, induced an irreversible dissociation process, resulting in smaller particles (D_h = 10 nm), with a broader size distribution. Alkaline dissociation starts at pH 9.0 and, as shown in Fig. 1 *B*, the increase of pH enhances the dissociation rate. In the pH range 9.0–10.1, the kinetics of dissociation was easily monitored by DLS. At pH 10.7, the dissociation kinetics was very fast (Fig. 1 *A*), not resolved by DLS. Fig. 2 presents the particle-size distributions at pH 7.0 (protein in its native form, D_h = 27 ± 1 nm), at pH 9.3 (protein partially dissociated) and pH 10.7 (dissociated protein, D_h = 10 ± 1 nm). The dissociated protein presents a higher polydispersion (Table 1). The average polydispersion indexes at pH 7.0 and pH 10.7 are 0.01 and 0.39, respectively. HbGp dissociation with the increase of pH is also evidenced with the decrease of $\langle D_h \rangle$ and the associated increase of polydispersion indexes. At pH >9.0, this process results in the appearance in solution of several species such as the dodecamer, tetramer, trimer, linker, and monomer, in addition to the remaining nondissociated protein in its original form. Gel filtration experiments described below show some evidence for this dissociation process. At pH >10.0, only smaller-molecular-weight species such as trimers, linkers, and monomers, appear in solution (Fig. 2).

Kaufman and co-workers (32) have demonstrated that the alkaline dissociation of HbLt provides a complex mixture.

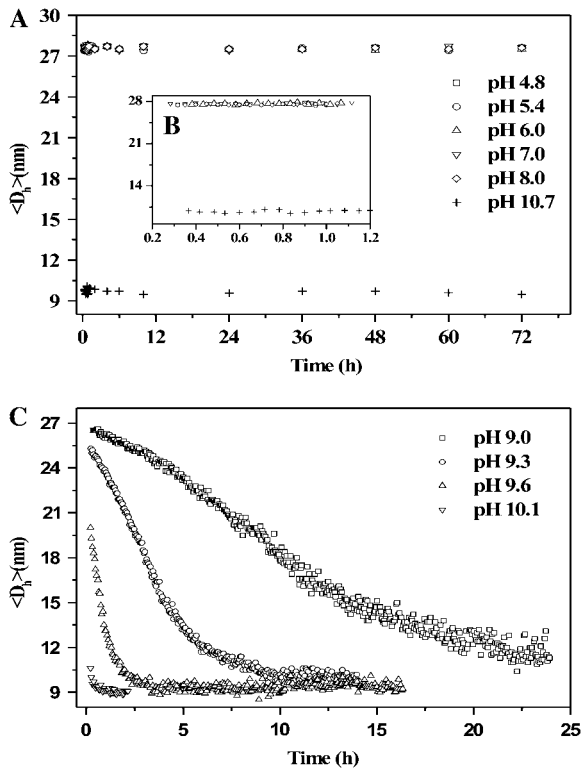

FIGURE 1 Variation of the hydrodynamic diameter (D_h) as a function of time for [HbGp] = 0.5-mg/ml at different pH values, in acetate-phosphate-borate buffer, 30 mM, at 25°C. (*A*) DLS measurements performed over a 72-h interval. (*B*) Initial kinetics for a 1.5-h interval. (*C*) DLS measurements performed over 24 h, showing the kinetics in the pH range 9.0–10.1 (see text for further details).

TABLE 1 *z*-Average hydrodynamic diameter, $\langle D_h \rangle$, average diffusion coefficient, D_Z, and polydispersity index obtained from analysis of DLS data for extracellular hemoglobin of *G. paulistus* in the oxy-form at different pH values

pH	$\langle D_h \rangle$ (nm)	D_Z (m^2/s) × 10^{-12}	Polydispersion (%)
4.8	28 ± 1	1.77	0.01
5.4	28 ± 1	1.78	0.01
6.1	27 ± 1	1.79	0.01
7.0	27 ± 1	1.79	0.01
8.0	27 ± 1	1.80	0.01
9.0	10 ± 1	4.92	0.30
9.3	10 ± 1	4.92	0.32
9.6	10 ± 1	4.92	0.31
10.1	10 ± 1	5.02	0.35
10.7	10 ± 1	5.12	0.39

In the pH range 4.8–8.0, the different values are obtained for a time interval of 1.5 h, whereas for pH values >9.0, the values correspond to the end of the kinetics.

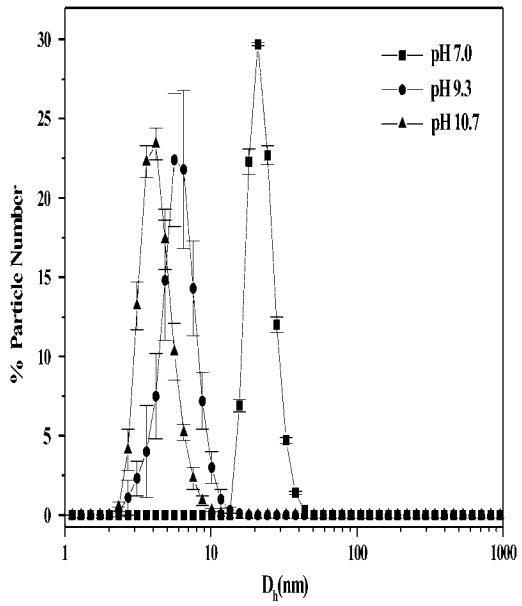

FIGURE 2 Particle-size distribution from DLS data of [HbGp] = 0.5 mg/ml in acetate-phosphate-borate, 30 mM, at pH 7.0, 9.3 and 10.7, obtained from data similar to those shown in Fig. 1 using the Cumulants method. The size distribution is obtained from the number of particles. The error bars represent the standard deviations of 15 different measurements. The error bars for the distribution at pH 9.3 are due to the very large change in size along the experiment. For pH 7.0 and 10.7, the time interval for measurement was 1.5 h. For pH 9.3 the time interval corresponds to the last 3 h of the kinetics measurement.

The dissociation at pH >8.0 results in different constituent subunits such as monomers, linkers, trimers, and dodecamers, whereas restoring the pH back to neutrality causes some reassociation of the dissociated protein. The gas-phase electrophoretic mobility molecular analysis spectra obtained for HbLt separated subunits made it possible to estimate the electrophoretic mobility diameter for several dissociated species. The electrophoretic mobility diameter values obtained for monomers, linkers, trimers, and dodecamers were, respectively, 4.2, 5.0, 6.3, and 10.5 nm. These results are in good agreement with our DLS data, where, for pH >9.0, a *z*-average particle diameter of 10 nm is observed, implying the possible presence of dodecamers in HbGp solution at this pH.

The value of $D_h = 27$ nm obtained for oxy-HbGp at pH 7.0 is similar to those obtained by small-angle x-ray scattering for extracellular HbLt ($D_{max} = 29$ nm (8,33)) and HbGp ($D_{max} = 30$ nm (34)). The D_{max} value corresponds to the maximum dimension of the scattering particle.

In this study, variation of HbGp concentration in the range 0.1–1.0 mg/ml at pH 7.0 (oligomeric stable native protein) showed identical DLS data, suggesting that in this concentration range no experimental artifacts take place due to protein-protein interactions or multiple scattering. Therefore, the concentration used in our study was chosen to be 0.5 mg/ml, the lowest concentration that gives a light-scattering signal suitable for reliable data treatment.

Gel exclusion chromatography and light-scattering intensities

Results from experiments of gel filtration size exclusion chromatography for samples of HbGp at 6.0 mg/ml concentration, and at three different pH values, are shown in Fig. 3. As can be seen from Fig. 3 *A*, at pH 7.0, the native protein is eluted at the exclusion volume of the column giving a single very sharp peak (Fraction I). This is consistent with previous observations of significant oligomeric stability at neutral pH, and also with the DLS data presented here (Fig. 1). Alkalization of the protein solution leads to a significant reduction of the native protein peak eluted at $V/V_0 = 1$, and a simultaneous observation of several peaks corresponding to species of lower molecular weight (Fig. 3, *B* and *C*). Fraction V in the chromatograms presented in these figures corresponds to very pure monomer, *d*, as characterized recently by MALDI-TOF MS (10). Fractions II and III are probably associated with heme containing aggregates, as seen by the high values of the ratio of absorbances at 415 nm and 280 nm. We believe there is a significant amount of trimers, maybe some dodecamers, and some monomers included in these fractions. Further work is under way to completely elucidate this point. Finally, fraction IV is probably rich in linker subunits, since the optical absorption at 415 nm associated to

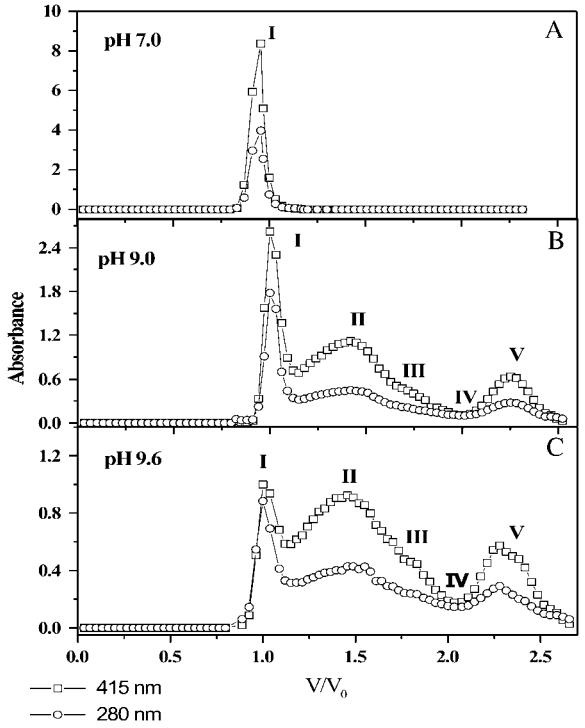

FIGURE 3 Gel filtration Sephadex G-200 chromatograms of [HbGp] = 6.0 mg/ml solutions in Tris-HCl 0.1 M, pH 7.0 (*A*), pH 9.0 (*B*) and pH 9.6 (*C*). Detection wavelengths are 280 nm (*circles*) and 415 nm (*squares*). Roman numerals I–V correspond to different species obtained for alkaline dissociation (see text). All chromatograms were obtained at 25°C.

the hemes is quite low, comparable to the absorption at 280 nm. In Fig. 4, LSIs are shown for the fractions obtained in the chromatograms in Fig. 3. It should be noted that the high LSI for fraction I (Fig. 3), associated with the native protein, is consistent with the maintenance of the oligomeric non-dissociated structure corresponding to a particle of maximum dimension around 30 nm (34), which agrees with the DLS data presented here (Fig. 1). The significant reduction of scattering for the remaining fractions in Fig. 3 is due to the dissociation of the protein exposed to alkaline medium. The scattering intensity depends on both the size of the aggregates and their concentration. Since the size dependence occurs as the square of the particle volume, we can conclude that the particle size of the species in fractions II–V is significantly smaller compared to the native protein, consistent with our DLS data at alkaline pH (Figs. 1 and 2) and with the results reported in Kaufmann et al. (32) for HbLt.

Dissociation kinetics by DLS

The dissociation kinetics is slow at pH 9.0 (5.6×10^{-5} s^{-1} (Table 2)), lasting ~24 h. The dissociation rate progressively increases at higher pH values (138×10^{-5} s^{-1} at pH 10.1, Table 2), at pH 10.7 going outside of the timescale at which it can be quantified by DLS. The values of D_h, diffusion coefficient, and polydispersion for HbGp at different pH values are presented in Table 1. In the pH range 4.8–8.0, the different values are obtained over a time interval of 1.5 h, whereas for pH values >9.0, the values correspond to the end of the kinetics. The *z*-average hydrodynamic diameter, $\langle D_h \rangle$, and the diffusion coefficient (obtained from the Stokes-Einstein equation (Eq. 1 in this article)) do change in the pH range between 8.0 and 9.0. The experimental data of the kinetics experiments shown in Fig. 1 were used to obtain the corresponding diffusion coefficients. Fig. 5 shows the experimental results together with the fittings of the kinetic curves to Eq. 5. The rate constants and diffusion coefficients are collected together in Table 2.

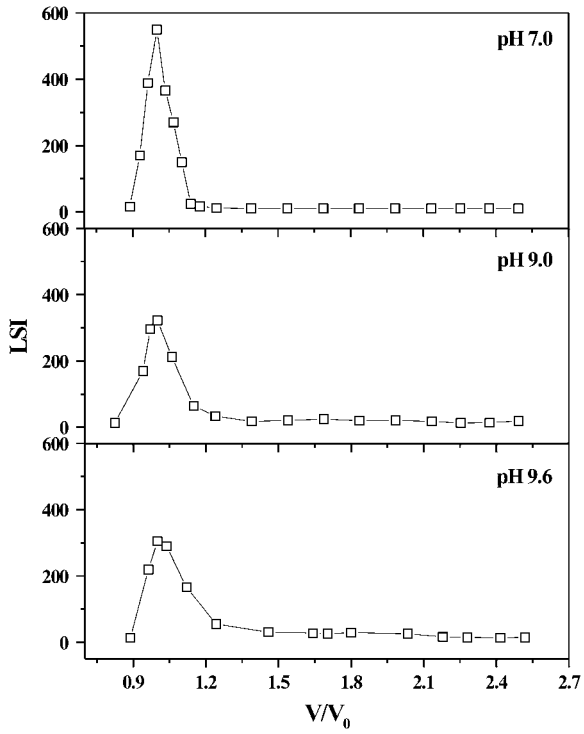

FIGURE 4 Light scattering intensity (LSI) of HbGp obtained from gel filtration chromatography in Sephadex G-200 chromatograms, corresponding to data shown in Fig. 3. Samples were monitored measuring the intensity at 90° in the fluorimeter with excitation and emission wavelengths of 350 nm (see text for details).

A monoexponential behavior was observed at pH 9.0, and this is due to the fact that the hemoglobin is, probably, in a more stable form as compared to more alkaline pH. The light-scattering intensities at pH 7.0 and 8.0 have higher values as a consequence of the maintenance of the protein native structure, without dissociation into smaller oligomeric fractions. Above pH 9.0, $\langle D_h \rangle$ decreases gradually. This decrease is related to the dissociation of the oligomeric structure into smaller protein subunits promoted by medium alkalization. In fact, $\langle D_h \rangle$ decreases from 27 nm to 10 nm, which suggests complete hemoglobin dissociation into trimers, linkers, and monomers.

A significant increase in rate constant was observed with increasing pH (Table 2): at pH 10.1, $k = (138 \pm 20) \times 10^{-5}$ s^{-1}, which is a factor of 28 higher than that at pH 9.0, $k = (5.06 \pm 0.06) \times 10^{-5}$ s^{-1}. All experimental curves were best fitted by Eq. 5. The overall process could be fitted adequately by the model in Eqs. 2–4 and the Appendix, based on a monoexponential dissociation kinetic. However, intermediate species are expected to be present in this dissociation equilibrium; our DLS data did not allow the determination of the rate constant associated to the intermediate step. Other than that, the value of k (rate constant) obtained in this study is related to all phases, or to the limiting step of the simple dissociation model proposed above.

Recent SAXS studies have also found that at pH 9.0, hemoglobin dissociation takes place (34). Intense oligomeric dissociation that occurs at pH 9.0, separating the protein fractions into trimers and monomers, was also considered as the main factor responsible for the biphasic nature in the autoxidation kinetics of HbGp (35).

Melting curves

Fig. 6 shows the ''melting curves'' reporting the values of D_h as a function of temperature for HbGp at different pH values. The rate of temperature change and the time spent at each temperature are described in Methods. Dissociation kinetics as a function of temperature was not investigated in this study. In Fig. 6 *A*, it can be seen that in the pH range 4.8–6.1, the increase in temperature does not induce HbGp dissociation. For values of pH 5.4 and 6.1, close to and above,

TABLE 2 Kinetic constants for dissociation of HbGp at different pH values obtained from the DLS data at 25°C

	pH			
Parameters*	9.0	9.3	9.6	10.1
k ($\times 10^{-5}$ s^{-1})	5.06 ± 0.06	16.5 ± 0.2	48 ± 2	138 ± 20
D_∞ ($\times 10^{-12}$ m^2s^{-1})	4.92	4.92	5.269 ± 0.008	5.43
X_o (s)	−31530 ± 944	−10330 ± 301	−5628 ± 323	−3430 ± 669
R^2	0.973	0.992	0.942	0.816
Experimental points	463	298	297	35

*See definition of parameters in the Appendix. X_0 corresponds to a time shift of the origin and R^2 is the correlation coefficient of the fit. The values $M_p = 3.1 \times 10^6$ Da, $D_p = 1.8 \times 10^{-12}$ m^2 s^{-1}, and $B = 1.33 \times 10^{11}$ Da^2 were used in all the fits to the experimental data.

respectively, the acid isoelectric point (pI) of this class of hemoglobins, HbGp denatures at $T = 55$°C, forming aggregates and precipitating. D_h values at temperatures below 55°C are ~27 ± 1 nm, almost the same as under native conditions. At pH 4.8, which is close to the pI for HbGp (pI = 5.5, assumed similar to that of HbLt (36)), the protein denaturation occurs at a lower temperature (52°C), without the formation of large aggregates and precipitation. Maximum $\langle D_h \rangle$ values above 52°C at pH 4.8 (260 nm) are lower than those at pH 6.1 and 5.4, which are 2650 and 3000 nm, respectively. The observed process was essentially irreversible, as can be deduced from the unchanged value of the hydrodynamic diameter obtained after cooling the sample back to 20°C after the denaturation (data not shown).

Fig. 6 *B* shows that at pH 7.0, where HbGp is very stable, the temperature does not induce the dissociation of the protein, but when a high temperature is reached (52°C), the denaturation of the protein occurs, forming a complex of $\langle D_h \rangle = 65$ nm. Probably, this value is underestimated since at the maximum temperature reached in the experiment, 65°C, the aggregate dimensions seem not to have reached a constant value. As mentioned above, a critical temperature was defined at 52°C and pH 7.0, where the scattering-particle dimension changed drastically. Although the curves at pH 4.8 and pH 7.0 display the same behavior, at pH 4.8, apparently, a larger complex ($\langle D_h \rangle = 260$ nm) is formed. However, since the aggregate dimension is underestimated at pH 7.0, its

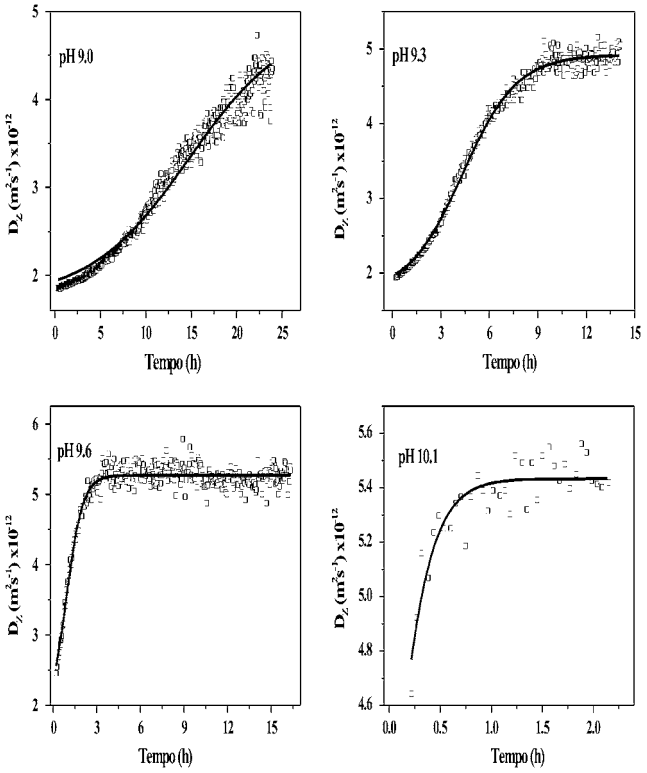

FIGURE 5 Dissociation kinetic decays and fits of oxy-hemoglobin of *G. paulistus*. DLS data were monitored as a function of time in acetate-phosphate-borate buffer, 30 mM, at different pH values (9.0, 9.3, 9.6, and 10.1), with $T = 25$°C and [HbGp] = 0.5 mg/ml. DLS kinetic decays were fitted to Eq. 5 to obtain the characteristic k (rate constant) values. All parameters from the fits are presented in Table 2 (see text).

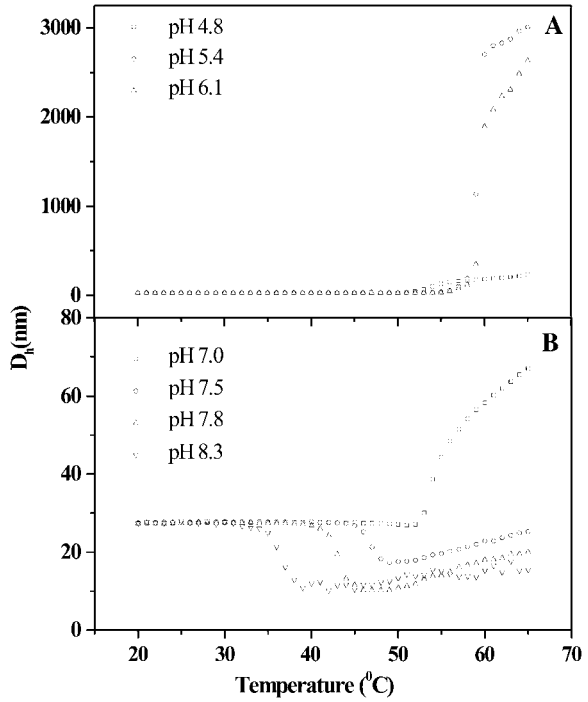

FIGURE 6 Effects of temperature on HbGp hydrodynamic radius at different pH values. [HbGp] = 0.5 mg/ml, in acetate-phosphate-borate buffer, 30 mM, at acid (*A*) and alkaline (*B*) pH values. Critical parameters (temperatures and sizes) are presented in Table 3.

upper limit could well be the same as that observed for pH 4.8. Furthermore, at higher pH values (in the range 7.5–8.3), where no significant alkaline protein dissociation is observed at room temperature, the increase of temperature causes the protein to dissociate before it has a chance to denature. The native protein with a D_h of 27.0 nm transforms into smaller particles with lower D_h values. A higher value of pH corresponds to a lower temperature at which the protein is seen to dissociate. Critical temperatures for dissociation and denaturation are shown in Table 3. At pH 7.0, and above 52°C, an increase of $\langle D_h \rangle$ is observed, whereas in the pH range 7.5–8.3, a decrease of $\langle D_h \rangle$ is associated with the temperature-induced protein dissociation, followed by an increase of $\langle D_h \rangle$, which is gradual and starts at a higher temperature, compared to the temperature for protein dissociation. It is worthy of notice that in Table 3, temperatures T_{diss} and T_{den} correspond to the beginning of the dissociation and denaturation processes, respectively. It is quite possible that the dissociation is not complete and that the beginning of denaturation overlaps with dissociation. Our data in Table 3 of T_{diss} as a function of pH are consistent with the data on pH stability shown in Fig. 1: as pH increases from 7.5 to 8.3, T_{diss} decreases from 44°C to 32°C, which is close to the temperature of 25°C used in our DLS kinetic experiments (Fig. 5). The values of $\langle D_h \rangle$ at the highest temperature (65°C) are higher at pH 7.0 (minimum of 65 nm), compared to the more alkaline pH range 7.5–8.3 (25–16 nm). This further indicates that temperature-induced protein dissociation is an irreversible process. Support for this conclusion also comes from the fact that lowering the temperature back to 25°C after heating to 65°C does not change the final value of $\langle D_h \rangle$.

Bonafe and co-workers (37), studying the reassembly mechanism of HbGp, argue that the irreversibility of protein dissociation is due to defective intermediate forms. These authors propose that after dissociation, the dissociated species undergo a conformational change that precludes an efficient subunit reassociation. Probably, this difficulty with reassembly is a consequence of the decrease in interchain contacts, especially those of electrostatic nature, as a function of the alteration of protein spatial arrangement. Cioni and Strambini (38) also proposed that conformational changes play a direct role in inhibiting subunit reassociation, implying the irreversibility of the protein dissociation. This would explain also why nonproteic factors—such as calcium ions, which bind, typically, to carboxylates, and glycerol—can promote, in some cases, a small oligomeric reassociation (5,37) by improving the intersubunit connections. Calcium ion, for example, being a metallic coordination center, induces the formation of various contacts between basic sites in the protein, which were eliminated upon the protein conformational changes associated with the dissociation process. This originates a ''template effect'' favoring the partial reorganization of the giant hemoglobin. This proposal is in agreement with a study by Rousselot and co-workers (39), who suggest that intersubunit contacts between extracellular hemoglobins, which would involve hydrogen bonds and salt bridges, are essential to form and to hold intact the complex quaternary structure. Studies focusing on the dissociation process of HbLt demonstrated that, in the absence of divalent cations, the reassociation was rather limited, generally $<10\%$ (40). Moreover, Kuchumov and co-workers studied the role of linkers in the reassembly of HbLt. They found that the four different linker subunits of HbLt are able to self-aggregate at neutral pH, originating dimers and higher-order multimers. The binary and ternary combinations and the nativelike mixture exhibited an extensive aggregation involving both heme-containing and nonheme (linker) subunits (41). This subunit aggregation is certainly a strong limitation for the reassembly of the native oligomeric protein. Furthermore, the strong dependence of protein dissociation on the ligand and valence state of the heme iron is well established, and the ferric species is quite unstable toward dissociation, as compared to the ferrous species (4,42). Heme autoxidation would inhibit the process of subunit reassociation.

In this way, the results presented here demonstrate that HbGp is sensitive to temperature, which seems to be an effective denaturation factor for this hemoglobin. The significant modification of the subunit tertiary structure would decrease the interchain contacts, precluding the reassociation process and making the dissociation process irreversible.

TABLE 3 Sizes and critical temperatures associated with the effects of temperature on oxy-HbGp *z*-average hydrodynamic diameter ($\langle D_h \rangle$) at different pH values

pH	T_{diss} (°C)	$\langle D_h \rangle_{(diss)}$ (nm)	T_{Den} (°C)	$\langle D_h \rangle_{(den)}$ (nm)
4.8	—	—	50 ± 1	260 ± 20
5.4	—	—	55 ± 2	3000 ± 30
6.1	—	—	56 ± 2	2650 ± 27
7.0	—	—	52 ± 1	65 ± 6
7.5	44 ± 1	27 ± 1	49 ± 1	25 ± 1
7.8	39 ± 1	27 ± 1	46 ± 1	20 ± 1
8.3	32 ± 2	27 ± 1	40 ± 1	16 ± 1

Melting points were obtained from the data in Fig. 6. T_{diss}, critical dissociation temperature (beginning of the dissociation process); T_{den}, critical denaturation temperature (beginning of the denaturation process); $\langle D_h \rangle_{(diss)}$, *z*-average hydrodynamic diameter at the beginning of the dissociation; $\langle D_h \rangle_{(den)}$, *z*-average hydrodynamic diameter at the highest temperature, 65°C.

UV-Vis

UV-Vis optical absorption was used to follow the spectral changes of HbGp as a function of pH. The spectra shown in Fig. 7 *A* were recorded 2 h after the preparation of the sample, and those in Fig. 7 *C* after 24 h of incubation at the indicated pH. Spectral changes in the Soret, α, and β bands were not observed after incubation for those pH values where the protein is more stable (pH 6.1–8.4). In contrast, at pH values >9.0, we observed a decrease and broadening of the Soret band, as well as broadening of the two Q-bands and an in-

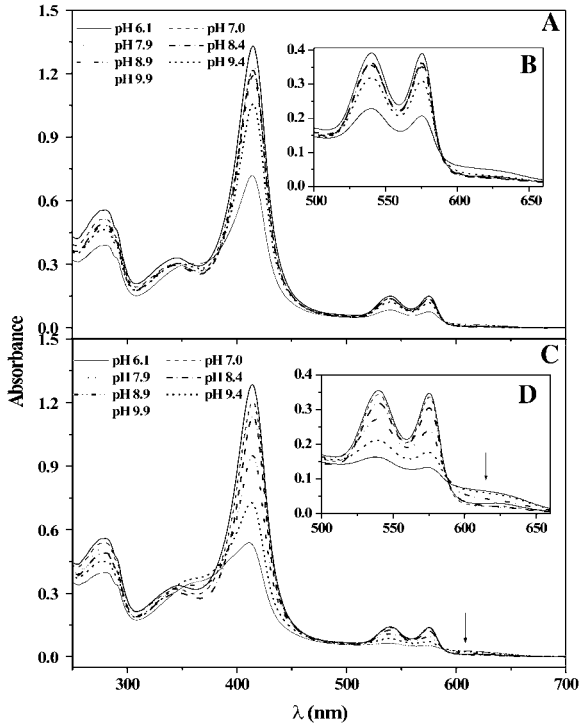

FIGURE 7 Optical absorption spectra of oxy-HbGp native protein in the pH range 6.1–9.9 showing the changes on the Soret band (*A* and *C*), and on the Q and LMCT band regions (*B* and *D*). These spectra correspond to measurements for the samples 1.5–2 h after preparation (*A* and *B*) and after 24 h of incubation (*C* and *D*).

crease of the ratio between their intensities (change in relative intensities). This intensity change of the Soret band and the two Q-bands could be an indication that an autoxidation process takes place, leading to the oxidation of the ferrous center. The appearance of a broad ligand-to-metal charge transfer (LMCT) band centered around 620 nm, characteristic of a ferric pentacoordinated species, is observed (Fig. 7 *C*, *arrow*). The coexistence of two species in equilibrium is observed, where one of them is a pentacoordinated species, which is also characterized by a lower-intensity Soret band shifted to the blue (26,27). The electronic absorption spectra obtained for different pH values indicate the oxidation at alkaline pH >9.0. In summary, the spectral behavior observed for HbGp as a function of pH (Fig. 7) is consistent with the autoxidation process that occurs at pH values >9.0.

In the Fig. 7 insets (Fig. 7, *B* and *D*), the region corresponding to the Q-bands (500–660 nm) and to the LMCT band (usually >600 nm) is enlarged for clarity of presentation. In the range pH 8.9–9.9, a significant decrease in absorption at the Soret band maximum (415 nm) is observed. At pH values equal to 8.9 and 9.9, a decrease of the Soret band intensity of 20 and 30%, respectively, takes place. Spectral changes in the pH range 6.1–8.4 are quite a bit smaller (a decrease of 4%).

At pH values >8.9, the decrease of intensity and blue shift of the Soret band, and the appearance of the characteristic LMCT band near 600–605 nm, indicate the formation of pentacoordinated heme at alkaline medium (43–45). The arrow in Fig. 7 *C* indicates the LMCT band. After 24 h of incubation at alkaline pH, the absorption spectra show the characteristic Q-bands of a hemichrome species with peaks centered at 535 and 565 nm (29), indicating the end of the autoxidation process as well as the ligand change in the sixth coordination site, which corresponds to to the coordination of distal histidine. These effects are characteristic for HbGp dissociation and autoxidation processes (26,35).

Autoxidation kinetics by UV-Vis

The kinetics of the autoxidation process was monitored for different pH values in the range 9.0–9.8, at $T = 25°C$ and 38°C. An increase in pH enhanced the autoxidation reaction rate at both temperatures. The rate constants as a function of pH, and at two different temperatures, are presented in Tables 4 and 5. The increase of pH and temperature leads to higher values of the rate constant, *k*.

Previous kinetic studies of the autoxidation of HbGp at pH 9.0 and 38°C have shown that the kinetics can be described by a biexponential behavior characterized by a fast and a slow rate constant. The fast rate constant was associated with the oxidation of hemes from the trimer (*abc*), whereas the slow process is associated with the oxidation of hemes from the monomer (*d*) (26).

In Fig. 8 *A* and Table 4, examples of kinetic curves and kinetic data obtained at 25°C are shown. As seen in Table 4, the kinetics at pH 9.0 and 9.3 is monoexponential, with a rate constant at pH 9.0 of $k = (1.8 \pm 0.2) \times 10^{-5}\ s^{-1}$. This value is a factor of 25 lower than the fast process and a factor of 5 lower than the slow process at pH 9.0 at 38°C (see Table 5 and Fig. 9). Starting at pH 9.6, the kinetics of HbGp autoxidation becomes biexponential (see Fig. 8 *A*) and the rate constant for the fast process increases at pH 9.8 almost 10-fold as compared to the value at pH 9.0 (Table 4 and Fig. 9).

On the other hand, at 38°C, the kinetics is biexponential in the whole pH range, in agreement with previous observations at pH 9.0 (26). It is worthy of notice that at 38°C, the contribution of the fast process in the kinetics at pH 9.0 and 9.3 is close to 100% (Table 5 and Fig. 9), implying a small con-

TABLE 4 Kinetic constants for the autoxidation of HbGp at 25°C

pH	k_{obs1} ($\times 10^{-5}\ s^{-1}$)	k_{obs2} ($\times 10^{-5}\ s^{-1}$)	$\Delta A_1 \times 10$	$\Delta A_2 \times 10$	$\%\Delta A_1$
9.0	1.8 ± 0.2		7.1 ± 0.6		
9.3	3.54 ± 0.04		7.1 ± 0.2		
9.6	10 ± 2	0.88 ± 0.02	5.1 ± 0.2	2.4 ± 0.2	68 ± 4
9.8	13.2 ± 0.3	1.03 ± 0.07	5.5 ± 0.4	2.9 ± 0.2	65 ± 5

k_{obs1} and k_{obs2} correspond to the fast and slow processes, respectively. ΔA_1 and ΔA_2 correspond to the amplitudes of the two processes. $\%\Delta A_1$ corresponds to the contribution of the fast process, $(\Delta A_1/(\Delta A_1 + \Delta A_2)) \times 100\%$.

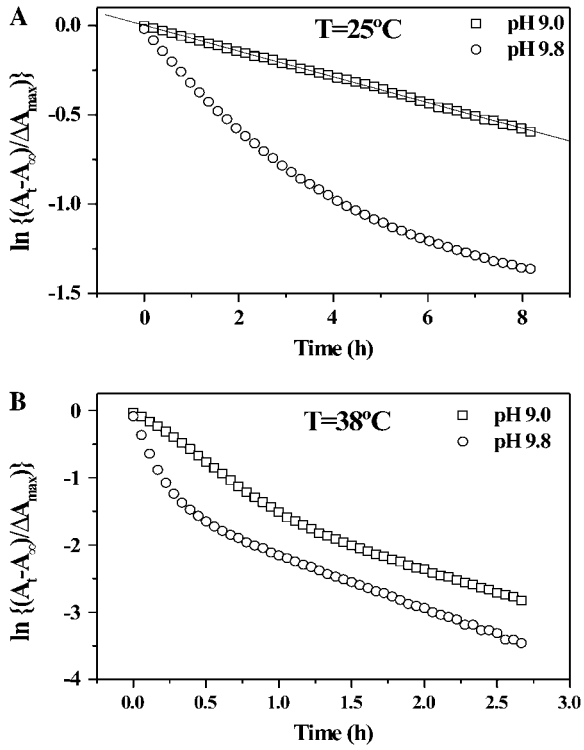

FIGURE 8 Kinetic curves corresponding to the autoxidation of HbGp in acetate-phosphate-borate buffer, 30 mM, at different pH values, at temperatures $T = 25°C$ (*A*) and $T = 38°C$ (*B*), at [HbGp] = 0.5 mg/ml. At pH 9.0, in *A*, the kinetics is monoexponential. Under all other experimental conditions, the decay is biexponential (see text for details).

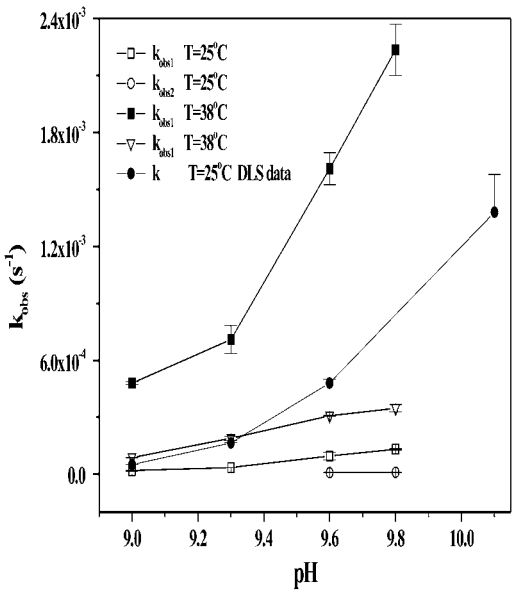

FIGURE 9 Rate constants, k_{obs}, at pH values 9.0, 9.3, 9.6, and 9.8, obtained from the autoxidation kinetics decays of oxy-HbGp 0.5 mg/ml. The absorbance at 415 nm was monitored as a function of time in acetate-phosphate-borate, 30 mM, at different pH values, at $T = 25°C$ and $T = 38°C$. Kinetic constants, *k*, from DLS data shown in Fig. 3 are also included for comparison.

tribution of the slow process, which does not appear at 25°C for these pH values (single exponential, Table 4 and Fig. 9).

It is also interesting to compare the rate constants obtained from DLS experiments (Table 2) with those for autoxidation measurements (Table 4). The values of *k* in DLS experiments are a factor of 2.7–4.8 higher than those from autoxidation. Clearly, in autoxidation experiments, the kinetics monitors the accessibility of the hemes upon their exposure to the solvent, especially to water and hydroxyl ligands capable of inducing changes in the iron vicinity. As mentioned above, this process is linked to the maintenance of the overall oligomeric protein structure, and DLS is sensitive in the first place to the average sizes of the scattering particles in solution.

Our data suggest, therefore, that dissociation precedes the autoxidation, since the values of *k* from DLS (Table 2) are higher than those from UV-Vis (Table 4). The process that prevails initially is the oligomeric dissociation, which initiates, in the sequence, a more pronounced autoxidation due to the higher water solvent accessibility in the heme pocket, which explains the higher rate constants obtained by DLS data compared with the values from UV-Vis. However, after an initial autoxidation process, a kind of cooperative effect should occur due to the well-known lower oligomeric stability of the ferric species compared with the oxy-form in giant extracellular hemoglobins (5,42). A sequence of events can then be proposed in the following order: 1), initial dissociation, followed by 2), autoxidation, and, further, 3), dissociation. Therefore, at the first stage, the initial dissociation process induced by the medium perturbations prevails; at the second stage, the autoxidation process takes place; and at the third stage, further dissociation due to the lower oligomeric stability of the oxidized species is observed.

The need for a biexponential fit at more alkaline pH values is probably related to the simultaneous occurrence of the dissociation and autoxidation processes, as observed from the alteration of the autoxidation kinetics in the absence of dissociation. At higher temperatures this effect is manifested even at lower pH values, which is in good agreement with the melting plots obtained from DLS. Apparently, the reverse effect (of autoxidation upon dissociation kinetics) is not so relevant, as observed from the DLS plots from an equation based on a monoexponential dissociation kinetics.

TABLE 5 Kinetics constants for the autoxidation of HbGp at 38°C

pH	k_{obs1} ($\times 10^{-4}$ s^{-1})	k_{obs2} ($\times 10^{-4}$ s^{-1})	$\Delta A_1 \times 10$	$\Delta A_2 \times 10$	$\%\Delta A_1$
9.0	4.80 ± 0.06	0.88 ± 0.01	5.3 ± 0.1	0.11 ± 0.2	98 ± 2
9.3	7.0 ± 0.7	1.9 ± 0.1	4.8 ± 0.1	0.10 ± 0.1	98 ± 1
9.6	16.0 ± 0.8	3.10 ± 0.01	4.1 ± 0.2	1.8 ± 0.3	69 ± 3
9.8	22.0 ± 1.0	3.5 ± 0.2	3.8 ± 0.4	2.0 ± 0.1	65 ± 5

k_{obs1} and k_{obs2} correspond to the fast and slow processes, respectively. ΔA_1 and ΔA_2 correspond to the amplitudes of the two processes. $\%\Delta A_1$ corresponds to the contribution of the fast process, $(\Delta A_1/(\Delta A_1+\Delta A_2)) \times 100\%$.

Our kinetic data suggest that the scattering particles in solution (a quite stable oligomeric structure at pH 7.0) dissociate at alkaline pH, starting at pH 9.0, into dodecamers, tetramers, trimers, linkers, and monomers, with a faster rate compared to that of iron autoxidation at 25°C. There is also support for oligomeric dissociation at alkaline pH >9.0 from the gel filtration chromatography data presented above, as well as from previous MALDI-TOF MS results (10). Since the k values differ by a factor of 3–5, our results are consistent with previous studies suggesting that autoxidation and oligomeric dissociation are intimately associated processes, capable of enhancing one another (5,26,27).

CONCLUSIONS

In this work, the stability of the extracellular HbGp was studied in terms of both alkaline pH dissociation and temperature effects. DLS results show that the protein oligomeric structure is quite stable in the pH range 4.8–8.0, undergoing pH-dependent dissociation above pH 9.0. The hydrodynamic diameter, D_h, is 27 ± 1 nm in the pH range 4.8–8.0, decreasing to 10 ± 1 nm at pH 10.7. The kinetics of dissociation was monitored in the pH range 9.0–10.1, at 25°C, showing a monoexponential behavior for the average diffusion coefficient on the basis of a simple model for the dissociation (Eqs. 2–4 and the Appendix). This is certainly a simplified model, which is justified on the basis of previous work on MALDI-TOF MS characterization of HbGp subunits (10). The rate constants for dissociation varied in the range 5–138 $\times 10^{-5}$ s^{-1}, increasing for higher pH values. DLS studies as a function of temperature show that the protein is quite stable at acid pH, undergoing denaturation above 55°C. In the pH range 7.5–8.3, the HbGp undergoes dissociation at temperatures in the range 32–45°C, the lower temperature corresponding to the higher pH. The dissociation is accompanied by denaturation at a temperature 8–10°C higher. At pH 7.0, dissociation is not observed and denaturation occurs at 52°C, followed by an increase in D_h to 65 nm.

Kinetics of HbGp autoxidation was monitored in the pH range 9.0–9.8 at 25°C and 38°C. At 25°C and pH 9.0 or 9.3, the kinetics is monoexponential, becoming biexponential at higher pH values. The rate constants vary in the range (1.8–13.2) $\times 10^{-5}$ s^{-1}, being higher at the more alkaline pH. They are a factor of 3–5 lower compared to kinetics monitored by DLS. At 38°C, the kinetics is biexponential in the whole pH range. We conclude that the dissociation monitored by DLS is faster compared to the autoxidation of heme, affecting the autoxidation kinetics. Although the two processes of oligomeric dissociation and heme autoxidation are interdependent for this class of hemoglobins, the reverse effect, of autoxidation upon oligomeric dissociation, seems to be less pronounced, since a monoexponential dissociation kinetics is always observed by DLS. This work shows that DLS can be used to follow, quantitatively and in real time, the kinetics of changes on the oligomerization of biologic complex supramolecular systems. The characterization of the stability of HbGp and of the pH- and temperature-induced destabilization of its quaternary structure, as well as the reciprocal effects of temperature on pH stability and pH on temperature stability, are of key importance for the development of mimetic systems of this protein and other erythrocruorins to be used as artificial blood substitutes.

APPENDIX

In a polydisperse sample, the value of the average diffusion coefficient, D_Z, is given by (22)

$$D_Z = \frac{\sum M_i^2 n_i D_i}{\sum M_i^2 n_i}, \tag{A1}$$

where D_i, M_i, and n_i refer to the diffusion coefficient, molecular weight, and concentration, respectively, of the different scattering particles in the sample. For the species involved in the dissociation equilibrium described by Eqs. 2–4, we have

$$D_Z = \frac{M_p^2 n_p D_p + M_{abc}^2 n_{abc} D_{abc} + M_d^2 n_d D_d + M_L^2 n_L D_L}{M_p^2 n_p + M_{abc}^2 n_{abc} + M_d^2 n_d + M_L^2 n_L}. \tag{A2}$$

The subscripts p, abc, d, and L refer to the integer HbGp protein, trimer, monomer, and linker, respectively. Considering the dissociation stoichiometry, it is known that $n_{abc} = n_d = n_L$. Therefore,

$$D_Z = \frac{M_p^2 n_p D_p + n_{abc}(M_{abc}^2 D_{abc} + M_d^2 D_d + M_L^2 D_L)}{M_p^2 n_p + n_{abc}(M_{abc}^2 + M_d^2 + M_L^2)}. \tag{A3}$$

Assuming a monoexponential dissociation kinetic with a rate constant k, and attending to the dissociation of each integer protein in 36 abc, d, or L units,

$$D_Z = \frac{M_p^2 D_p e^{-kt} + 36(1 - e^{-kt})(M_{abc}^2 D_{abc} + M_d^2 D_d + M_L^2 D_L)}{M_p^2 e^{-kt} + 36(1 - e^{-kt})(M_{abc}^2 + M_d^2 + M_L^2)} \tag{A4}$$

and

$$D_Z = \frac{(M_p^2 D_p - 36(M_{abc}^2 D_{abc} + M_d^2 D_d + M_L^2 D_L))e^{-kt} + 36(M_{abc}^2 D_{abc} + M_d^2 D_d + M_L^2 D_L)}{(M_p^2 - 36(M_{abc}^2 + M_d^2 + M_L^2))e^{-kt} + 36(M_{abc}^2 + M_d^2 + M_L^2)}. \tag{A5}$$

By defining A and B as

$$A = 36(M_{abc}^2 D_{abc} + M_d^2 D_d + M_L^2 D_L) \tag{A6}$$

$$B = 36(M_{abc}^2 + M_d^2 + M_L^2), \tag{A7}$$

this equation can be simplified as

$$D_Z = \frac{(M_p^2 D_p - A)e^{-kt} + A}{(M_p^2 - B)e^{-kt} + B}. \quad \text{(A8)}$$

The limit value of the average diffusion coefficient, D_∞, can be easily obtained from the experimental data. Based on the previous equation,

$$D_\infty = \lim_{t\to\infty} D_Z = \frac{A}{B}. \quad \text{(A9)}$$

Consequently,

$$D_Z = \frac{(M_p^2 D_p - BD_\infty)e^{-kt} + BD_\infty}{(M_p^2 - B)e^{-kt} + B}, \quad \text{(A10)}$$

which is identical to Eq. 5.

The authors thank Prof. Miguel Castanho (University of Lisbon, Lisbon, Portugal) for valuable discussions. The authors are also indebted to Mr. Ézer Biazin for excellent technical support with gel filtration experiments, and to Dr. Alessandra L. Poli for useful comments on UV-Vis data.

The authors are grateful to the Brazilian agencies Fundação de Amparo à Pesquisa do Estado de São Paulo, Conselho Nacional de Desenvolvimento Científico e Tecnológico, and Coordenadoria de Aperfeiçoamento de Pessoal do Ensino Superior and to the Portuguese Fundação para a Ciência e Tecnologia - Ministério da Ciência, Tecnologia e Ensino Superior for partial financial support.

REFERENCES

1. Weber, R. E., and S. N. Vinogradov. 2001. Nonvertebrate hemoglobins: functions and molecular adaptations. *Physiol. Rev.* 81:570–611.
2. Royer, W. E., H. Zhu, T. A. Gorr, J. F. Flores, and J. E. Knapp. 2005. Allosteric hemoglobin assembly: diversity and similarity. *J. Biol. Chem.* 280:27477–27480.
3. Vinogradov, S. N. 2004. The stoichiometry of the four linker subunits of *Lumbricus terrestris* hemoglobin suggests an asymmetric distribution. *Micron.* 35:127–129.
4. Rousselot, M., E. Delpy, C. D. La Rochelle, V. Lagente, R. Pirow, J. Rees, A. Hagege, D. Le Guen, S. Hourdez, and F. Zal. *Arenicola marina* extracellular hemoglobin: a new promising blood substitute. 2006. *Biotechnol. J.* 1:333–345.
5. Zhu, H., D. W. Ownby, C. K. Riggs, N. J. Nolasco, J. K. Stoops, and A. F. Riggs. 1996. Assembly of the gigantic hemoglobin of the earthworm *Lumbricus terrestris*: roles of subunit equilibria, non-globin linker chains, and valence of the heme iron. *J. Biol. Chem.* 271:30007–30021.
6. Fushitani, K., and A. F. Riggs. 1991. The extracellular hemoglobin of the earthworm, *Lumbricus terrestris*: oxygenation properties of isolated chains, trimer, and a reassociated product. *J. Biol. Chem.* 266:10275–10281.
7. Costa, M. C. P., C. F. S. Bonafé, N. C. Meirelles, and F. Galembeck. 1988. Sedimentation coefficient and minimum molecular-weight of extracellular hemoglobin of *Glossoscolex paulistus* (Oligochaeta). *Braz. J. Med. Biol. Res.* 21:115–118.
8. Zal, F., B. N. Green, P. Martineau, F. H. Lallier, A. Toulmond, S. N. Vinogradov, and J. J. Childress. 2000. Polypeptide chain composition diversity of hexagonal-bilayer hemoglobins within a single family of annelids, the alvinellidae. *Eur. J. Biochem.* 267:5227–5236.
9. Krebs, A., P. Zipper, and S. N. Vinogradov. 1996. Lack of size and shape alteration of oxygenated and deoxygenated *Lumbricus terrestris* hemoglobin? *Biochim. Biophys. Acta.* 1297:115–118.
10. Oliveira, M. S., L. M. Moreira, and M. Tabak. 2007. Partial characterization of giant extracellular hemoglobin of *Glossoscolex paulistus*: a MALDI-TOF-MS study. *Int. J. Biol. Macromol.* 40:429–436.
11. Meirelles, N. C., B. Oliveira, E. de Paula, S. Marangoni, and G. M. Rennebeck. 1987. Erythrocruorin of *Glossoscolex paulistus* (oligochaeta, glossoscolecidae): dissociation at alkaline pH and its ligand properties as revealed by chemical, immunochemical and electronmicroscopy studies. *Comp. Biochem. Physiol.* 88A:337–379.
12. Martin, P. D., A. R. Kuchumov, B. R. Green, R. W. A. Oliver, E. H. Braswell, J. S. Wall, and S. N. Vinogradov. 1996. Mass spectrometric composition and molecular mass of *Lumbricus terrestris* hemoglobin: a refined model of its quaternary structure. *J. Mol. Biol.* 255:154–169.
13. Viana, E., C. H. T. P. Silva, M. Tabak, H. Imasato, and R. C. Garrat. 1998. A molecular model for the *d* chain of the giant hemoglobin from *Lumbricus terrestris* and its implications for subunit assembly. *Biochim. Biophys. Acta.* 1383:130–142.
14. Haas, F., A. Kuchumov, J. C. Taveau, N. Boisset, S. N. Vinogradov, and J. N. Lam. 1997. Three-dimensional reconstruction of native and reassembled *Lumbricus terrestris* extracellular hemoglobin. Localization of the monomeric globin chains. *Biochemistry.* 36:7330–7338.
15. Mouche, F., N. Boisset, and P. A. Penczek. 2001. *Lumbricus terrestris* hemoglobin: the architecture of linker chains and structural variation of the central toroid. *J. Struct. Biol.* 133:176–192.
16. Daniel, E., A. Lustig, M. M. David, and Y. Tsfadia. 2004. On the molecular mass of *Lumbricus* erythrocruorin. *Micron.* 35:131–132.
17. Kapp, O. H., G. Polidori, M. G. Mainwaring, A. V. Crewe, and S. N. Vinogradov. 1984. The reassociation of *Lumbricus terrestris* hemoglobin dissociated at alkaline pH. *J. Biol. Chem.* 259:628–639.
18. Strand, K., J. E. Knapp, B. Bhyravbhatia, and W. E. Royer Jr. 2004. Crystal structure of the hemoglobin dodecamer from *Lumbricus* erythrocruorin: allosteric core of giant annelid respiratory complexes. *J. Mol. Biol.* 344:119–134.
19. Royer, W. E., H. Sharma, K. Strand, J. E. Knapp, and B. Bhyravbhatla. 2006. *Lumbricus* erythrocruorin at 3.5 Å resolution: architecture of a megadalton respiratory complex. *Structure.* 14:1167–1177.
20. Dathe, M., K. Gast, D. Zirwer, H. Welfle, and B. Mehlis. 1990. Insulin aggregation in solution. *Int. J. Pept. Protein Res.* 36:344–349.
21. Banachowicz, E. 2006. Light scattering studies of proteins under compression. *Biochim. Biophys. Acta.* 1764:405–413.
22. Santos, N. C., and M. A. R. B. Castanho. 1996. Teaching light scattering spectroscopy: the dimension and shape of tobacco mosaic virus. *Biophys. J.* 71:1641–1650.
23. Santos, N. C., M. J. E. Pietro, A. Morna-Gomes, D. Betbeder, and M. A. R. B. Castanho. 1997. Structural characterization (shape and dimensions) and stability of polysaccharide/lipid nanoparticles. *Biopolymers.* 41:511–520.
24. Favilla, R., F. D. Signore, E. Dainese, M. Beltramini, and B. Salvato. 1998. Dissociation kinetics of hemocyanin from *Octopus vulgaris*. *Biochim. Biophys. Acta.* 1383:115–125.
25. Petta, V., J. Moradian-Oldak, S. N. Yannopoulos, and N. Bouropoulos. 2006. Dynamic light scattering study of an amelogenin gel-like matrix in vitro. *Eur. J. Oral Sci.* 114:308–314.
26. Poli, A. L., L. M. Moreira, M. Tabak, and H. Imasato. 2006. SDS (sodium dodecyl sulfate) effect on the autoxidation of the *Glossoscolex paulistus* giant extracellular hemoglobin: kinetic studies at pH 7.0 and 9.0. *Colloid Surf. B Biointerfaces.* 52:96–104.
27. Santiago, P. S., L. M. Moreira, E. V. de Almeida, and M. Tabak. 2007. Giant extracellular *Glossoscolex paulistus* hemoglobin (HbGp) upon interaction with cethyltrimethylammonium chloride (CTAC) and sodium dodecyl sulphate (SDS) surfactants: dissociation of oligomeric structure and autoxidation. *Biochim. Biophys. Acta.* 1770: 506–517.
28. Agustinho, S. C. M., M. H. Tinto, J. R. Perussi, M. Tabak, and H. Imasato. 1998. Fluorescence studies of extracellular hemoglobin of *Glossoscolex paulistus* in met form obtained from sephadex gel filtration. *Comp. Biochem. Physiol.* 118A:171–181.

29. Agustinho, S. C. M., M. H. Tinto, H. Imasato, T. T. Tominaga, J. R. Perussi, and M. Tabak. 1996. Spectroscopic studies of the met form of the extracellular hemoglobin from *Glossoscolex paulistus*. *Biochim. Biophys. Acta.* 1298:148–158.

30. Pecora, R. 1985. Dynamic Light Scattering. Plenum Press, New York.

31. Benjwal, S., S. Jayaraman, and O. Gursky. 2005. Electrostatic effects on the stability of discoidal high-density lipoproteins. *Biochemistry.* 44:10218–10226.

32. Kaufman, S. L., A. R. Kuchumov, M. Kazakevich, and S. N. Vinogradov. 1998. Analysis of a 3.6-MDa hexagonal bilayer hemoglobin from *Lumbricus terrestris* using a gas-phase electrophoretic mobility molecular analyzer. *Anal. Biochem.* 259:195–202.

33. Krebs, A., J. Lamy, S. N. Vinogradov, and P. Zipper. 1998. *Lumbricus terrestris* hemoglobin: a comparison of small angle x-ray scattering and cryoelectron microscopy data. *Biopolymers.* 45:289–298.

34. Gelamo, E. L., R. Itri, and M. Tabak. 2004. Small angle x-ray scattering (SAXS) study of the extracellular hemoglobin of *Glossoscolex paulistus*: effect of pH, iron oxidation state, and interaction with anionic SDS surfactant. *J. Biol. Chem.* 279:33298–33305.

35. Poli, A. L., L. M. Moreira, A. A. Hidalgo, and H. Imasato. 2005. Autoxidation studies of extracellular hemoglobin of *Glossoscolex paulistus* at pH 9: cyanide and hydroxyl effect. *Biophys. Chem.* 114: 253–260.

36. Fushitani, K., K. Higashiyama, M. Asao, and K. Hosokawa. 1996. Characterization of the constituent polypeptides of the extracellular hemoglobin from *Lumbricus terrestris:* heterogeneity and discovery of a new linker chain L4. *Biochim. Biophys. Acta.* 1292:273–280.

37. Bonafe, C. F. S., M. Villas-Boas, M. C. Suarez, and J. L. Silva. 1991. Reassembly of a large multisubunit protein promoted by nonprotein factors: effects of calcium and glycerol on the association of extracellular hemoglobin. *J. Biol. Chem.* 266:13210–13216.

38. Cioni, P., and G. B. Strambini. 1997. Pressure-induced dissociation of yeast glyceraldehyde-3-phosphate dehydrogenase: heterogeneous kinetics and perturbations of subunit structure. *Biochemistry.* 36:8586–8593.

39. Rousselot, M., D. Le Guen, C. Chabasse, and F. Zal. 2006. Native and subunit molecular mass and quarternary structure of the hemoglobin from the primitive *Branchiopod crustacean triops cancriformis*. *FEBS J.* 273:1582–1596.

40. Sharma, P. K., A. R. Kuchumov, G. Chottard, P. D. Martin, J. S. Wall, and S. N. Vinogradov. 1996. The role of the dodecamer subunit in the dissociation and reassembly of the hexagonal bilayer structure of *Lumbricus terrestris* hemoglobin. *J. Biol. Chem.* 271:8754–8762.

41. Kuchumov, A. R., J. C. Taveau, J. N. Lamy, J. S. Wall, R. E. Weber, and S. N. Vinogradov. 1998. The role of linkers in the reassembly of the 3.6 MDa hexagonal bilayer hemoglobin from *Lumbricus terrestris*. *J. Mol. Biol.* 289:1361–1374.

42. Riggs, A. F. 1998. Self-association, cooperativity and supercooperativity of oxygen binding by hemoglobins. *J. Exp. Biol.* 201:1073–1084.

43. Pietri, R., L. Granell, A. Cruz, W. de Jésus, A. Lewis, R. Leon, C. L. Cadilla, and J. L. Garriga. 2005. Tyrosine B10 and heme-ligand interactions of *Lucina pectinata* hemoglobin II: control of heme reactivity. *Biochim. Biophys. Acta.* 1747:195–203.

44. Gilles-Gonzalez, M. A., G. Gonzalez, and M. F. Perutz. 1994. Heme-based sensors, exemplified by the kinase FixL, are a new class of heme protein with distinctive ligand-binding and autoxidation. *Biochemistry.* 33:8067–8073.

45. Boffi, A., T. K. Das, S. D. Longa, C. Spagnuolo, and D. L. Rousseau. 1999. Pentacoordinate hemin derivatives in sodium dodecyl sulfate micelles: model systems for the assignment of the fifth ligand in ferric heme proteins. *Biophys. J.* 77:1143–1149.